



# Fractional Calculus & Applied Analysis

An International Journal for Theory and Applications

VOLUME 24, NUMBER 6 (2021)

(Print) ISSN 1311-0454  
(Electronic) ISSN 1314-2224

## RESEARCH PAPER

### CONVERGENCE RATE ESTIMATES FOR THE KERNELIZED PREDICTOR CORRECTOR METHOD FOR FRACTIONAL ORDER INITIAL VALUE PROBLEMS

Joel A. Rosenfeld<sup>1,§</sup>, Warren E. Dixon<sup>2</sup>

#### Abstract

This manuscript presents a kernelized predictor corrector (KPC) method for fractional order initial value problems, which replaces linear interpolation with interpolation by a radial basis function (RBF) in a predictor-corrector scheme. Specifically, the class of Wendland RBFs is employed as the basis function for interpolation, and a convergence rate estimate is proved based on the smoothness of the particular kernel selected. Use of the Wendland RBFs over Mittag-Leffler kernel functions employed in a previous iteration of the kernelized method removes the problems encountered near the origin in [11]. This manuscript performs several numerical experiments, each with an exact known solution, and compares the results to another frequently used fractional Adams-Bashforth-Moulton method. Ultimately, it is demonstrated that the KPC method is more accurate but requires more computation time than the algorithm in [4].

*MSC 2010:* 26A33, 65L05, 34A08

*Key Words and Phrases:* fractional ordinary differential equations; Adams Bashforth Moulton; reproducing kernel Hilbert spaces; Wendland radial basis functions

### 1. Introduction

Given the initial value problem involving the Caputo fractional derivative,  $D_*^q$  for  $q > 0$ ,

$$D_*^q y(s) = f(s, y(s)) \quad \text{such that} \quad \left. \frac{d^k}{ds^k} y \right|_{s=0} = y_0^k. \quad (1.1)$$

Here  $s \in [0, T] \subset \mathbb{R}$ ,  $k = 0, \dots, [q]$ , and  $[\cdot]$  is the largest integer less than or equal to  $q$ . The Caputo fractional derivative is defined as

$$D_*^q f(s) := \frac{1}{\Gamma(\alpha - q)} \int_0^s (s - \tau)^{\alpha - q - 1} \frac{d^\alpha}{d\tau^\alpha} f(\tau) d\tau,$$

where  $\alpha = [q]$ . An equivalent expression to that of (1.1) is given as a Volterra integral equation (cf. [4]):

$$y(s) = \sum_{k=0}^{[q]} \frac{s^k}{k!} y_0^{(k)} + \frac{1}{\Gamma(q)} \int_0^s (s - \tau)^{q-1} f(\tau, y(\tau)) d\tau. \quad (1.2)$$

The form given in (1.2) is more conducive to numerical methods than the form given in (1.1) and was leveraged in [4] to establish a fractional order Adams-Bashforth-Moulton (ABM) method. Unlike integer order IVPs, where it is possible to use only a small number of local samples to obtain an accurate estimation of a function's derivative, a history of  $f(\cdot, y(\cdot))$  over  $[0, s]$  must be curated to estimate the solution of a fractional IVP at  $s$ . The maintenance of an accurate approximation of the solution to (1.1) then becomes a matter of determining an effective method that is also computationally efficient. In [7], a predictor corrector method was developed that utilizes piecewise constant estimations of  $f$  for the predictor and a piecewise linear estimation of  $f$  for each corrector step. Further development of the ABM method for fractional order IVPs can be found in [5, 6], and the method is presented in the book [4]. The ABM method as conceived in [4] was modified in [11] for the development of a kernelized predictor corrector (KPC) method where the corrector term incorporates kernelized interpolation.

Kernelized interpolation allows for a flexible choice of interpolants, where each selected kernel function provides a different numerical method suited for functions in different function classes as in [14]. A major drawback of the kernelized method is that it is hard to achieve a comprehensible convergence rate across all kernel functions. In [11], the Mittag-Leffler RKHS was introduced where the kernel functions of that space are eigenfunctions of the Caputo fractional derivative, and [11] leveraged the Mittag-Leffler space for a KPC method. The Mittag-Leffler space received a deeper development as a RKHS in [12]. However, the Mittag-Leffler kernel functions suffer from a vertical asymptote at the origin, which interferes with the

generation of an accurate numerical method at the origin as demonstrated in [11]. This lack of continuous differentiability aligns with [4, Theorem 6.27] where continuous differentiability of solutions of fractional order initial value problems is guaranteed everywhere but the origin. The focus of [11] was the development of the Mittag-Leffler RKHS as a means to estimate a function's Caputo fractional order derivative, and does not provide convergence rate guarantees for the KPC when using the Mittag-Leffler kernel. Specifically, in [11], the convergence criteria for the kernelized numerical method is expressed in terms of a Hilbert space norm, rather than the convenient convergence rates in terms of the separation between time-steps,  $h$ , found in [4]. Moreover, the vertical asymptotes expressed by the basis functions at the origin cause numerical issues, where extremely large errors are obtained for small step-sizes in Figure 3 for the KPC method using the Mittag-Leffler kernel.

This manuscript establishes that a convergent rate estimate in terms of the step size can be extracted from the KPC method through the proper selection of kernel functions. In particular, existing results for interpolation by radial basis functions (RBFs) (cf. [3, 9, 14]) can be leveraged to yield convergence rate estimates for the KPC method. In addition, the use of the Wendland RBF as a kernel function for the KPC method avoids the difficulties introduced at the origin when using the Mittag-Leffler kernel functions and improves upon the performance of the KPC method using the Mittag-Leffler kernel function as demonstrated in Figure 3.

Section 2 reviews features of the Wendland RBFs that are pertinent for the present manuscript. Section 4 gives an outline of the KPC algorithm, and the corresponding convergence analysis is given in Section 5. After a discussion concerning implementation of the algorithm using the Wendland RBFs in Section 6, several numerical experiments are performed in Section 7 and the results are discussed in Section 8.

## 2. Review of the Wendland radial basis functions

Kernel functions and RBFs in particular are utilized throughout approximation theory and machine learning. A radial basis function is derived from a function,  $\Phi \in C(\mathbb{R}^n) \cap L^1(\mathbb{R}^n)$ , and given as  $K(x, y) = \Phi(\|x - y\|_2)$  where  $x, y \in \mathbb{R}^n$ . The most commonly used kernel function is that of the Gaussian RBF,  $K(x, y) = \exp(-\|x - y\|_2)$ . Corresponding to kernel functions are their native reproducing kernel Hilbert spaces, defined in [14] as follows.

**DEFINITION 2.1.** Given  $\Phi \in C(\mathbb{R}^n) \cap L^1(\mathbb{R}^n)$  the *native space* corresponding to  $\Phi$ ,  $\mathcal{N}_\Phi(\mathbb{R}^n)$ , consists of those functions  $g$  such that  $\frac{\hat{g}}{\sqrt{\hat{\Phi}}} \in L^2(\mathbb{R}^n)$ .

The native space,  $\mathcal{N}_\Phi(\mathbb{R}^n)$ , is a reproducing kernel Hilbert space with inner product  $\langle f, g \rangle_{\mathcal{N}_\Phi(\mathbb{R}^n)} := \left\langle \hat{f}/\sqrt{\hat{\Phi}}, \hat{g}/\sqrt{\hat{\Phi}} \right\rangle_{L^2(\mathbb{R}^n)}$  and kernel function  $K(x, y) = \Phi(\|x - y\|_2)$  such that  $\langle f, K(\cdot, y) \rangle_{\mathcal{N}_\Phi(\mathbb{R}^n)} = f(y)$  for all  $y \in \mathbb{R}^n$  and  $f \in \mathcal{N}_\Phi(\mathbb{R}^n)$  (cf. [14]).

The kernels featured in this manuscript are based on Wendland functions. For a function  $\phi : \mathbb{R} \rightarrow \mathbb{R}$  such that the mapping  $t \mapsto t\phi(t)$  is in  $L^1[0, \infty]$ , define  $\mathcal{I}\phi(\tau) := \int_\tau^\infty t\phi(t)dt$  (cf. [14]). Set  $\phi_p(\tau) := (\max\{0, (1 - \tau)\})^p$  and  $\phi_{d,r} = \mathcal{I}\phi_{[d/2]+r+1}$ . For  $d, r \in \mathbb{N}$ , the Wendland RBFs are defined as (c.f. [14])

$$K(x, y) = \Phi_{d,r}(x - y) := \phi_{d,r}(\|x - y\|_2).$$

The Wendland functions have several desirable features. The Wendland RBF,  $\Phi_{d,r}$ , is a positive definite RBF on  $\mathbb{R}^d$ , which means that linear combinations of translates of the Wendland RBFs can interpolate any finite collection of points. The function  $\Phi_{d,r}$  is compactly supported, a polynomial on its support, and has continuous derivatives of up to order  $2r$ . Finally, the native space corresponding to  $\Phi_{d,r}$  is norm equivalent to a Sobolev space, which means the native space is as general as that used for most well established numerical methods (cf. [8]). To facilitate the development of improved convergence rates, Theorem 2.1 is adapted and specialized from [14, Theorem 11.17] and establishes convergence rate guarantees of an approximation determined by interpolants in a native Hilbert space.\* In particular, the native space for the Wendland RBFs is the Sobolev space  $H^{d/2+k+1/2}(\mathbb{R}^n)$  (c.f. [14, Theorem 10.35]).

**THEOREM 2.1.** *For  $d, r \in \mathbb{N}$ , let  $\Phi_{d,r} = \phi_{d,r}(\|\cdot\|)$  be a Wendland RBF (cf. [14]). Further let  $I \subset \mathbb{R}$  be a compact interval. Let  $s_{f,X}$  be the RBF interpolant, determined by  $\Phi_{d,r}$ , to  $f$  in the RBFs native space over  $I$ ,  $N_{\Phi_{d,r}}(I)$ , and  $X = \{x_1, \dots, x_N\}$ . Fix  $\alpha \in \mathbb{N}_0$  ( $\alpha < k$ ). There exists constants  $C, h_0 > 0$  such that*

$$\left| \frac{d^\alpha}{dx^\alpha} f(x) - \frac{d^\alpha}{dx^\alpha} s_{f,X}(x) \right| \leq Ch_{X,I}^{r+1/2-\alpha} \|f\|_{N_\Phi(I)}$$

for all  $x \in I$  provided that  $h_{X,I} := \sup_{y \in I} \inf_{x \in X} \|x - y\| < h_0$ .

---

\* Each RKHS over  $X$  has uniquely defined function  $K : X \times X \rightarrow \mathbb{R}$  such that for any finite collection of points in  $X$ , say  $x_1, \dots, x_m$ , the Gram matrix  $(K(x_i, x_j))_{i,j=1}^m$  is positive definite. Moreover, for each such function there is a corresponding RKHS, which is denoted as the kernel function's native space (c.f. [14, Theorem 10.10] or [2]). For a radial basis function  $K(x, y) = \Phi(\|x - y\|)$  the native space is denoted by  $\mathcal{N}_\Phi(X)$  and  $\mathcal{N}_\Phi$  when the domain is understood.

There are two standard (and equivalent) representations for  $s_{f,X}$  given in Theorem 2.1. The most direct representation arises from the kernels as basis functions:

$$s_{f,X}(x) = \sum_{i=1}^N w_i \Phi_{d,r}(x - x_i). \tag{2.1}$$

The coefficients,  $w_i \in \mathbb{R}$ , are uniquely determined by the samples  $(x_i, f(x_i))$  and are determined by solving the matrix equation  $(\Phi_{d,r}(x_i - x_j))_{i,j=1}^N \mathbf{w} = \mathbf{f}$  where  $\mathbf{w} = (w_1, \dots, w_N)^T$  and  $\mathbf{f} = (f(x_1), \dots, f(x_N))^T$ . The second representation is given by

$$s_{f,X}(x) = \sum_{i=1}^N f(x_i) u_i^*(x), \tag{2.2}$$

where  $u_i^*(x) = \sum_{j=1}^N \tilde{u}_j \Phi_{d,r}(x - x_j)$  arise from the solution of the equation  $(\Phi_{d,r}(x_i - x_j)) \mathbf{u}_i = \mathbf{e}_i$  where  $\mathbf{u}_i = (\tilde{u}_1, \dots, \tilde{u}_N)^T$  and  $\mathbf{e}_i = (\delta_{i1}, \dots, \delta_{iN})^T$  resulting in  $u_i(x_j) = \delta_{ij}$  (here  $\delta_{ij}$  is the Kronecker delta function) (cf. [3, 14]). A key feature exploited in this manuscript of the cardinal functions,  $u_i^*$ , can be found in [3], as follows.

LEMMA 2.1 ([3]). *For uniformly spaced points,  $|\sum_{i=1}^N u_i^*(x)| \leq C\sqrt{N}$ , where  $C$  is a positive constant independent of  $x$  and  $N$ .*

### 3. Wendland RBFs for estimating Caputo fractional derivatives

As motivation for the KPC algorithm presented in Section 4, this section demonstrates that the Wendland RBFs can be leveraged to produce an estimate for a function’s fractional derivative without the drawbacks found using the Mittag-Leffler kernel function near the origin in [11].

The advantage of applying the Mittag-Leffler kernel functions to the problem of estimating a function’s fractional derivative arises from the eigenfunction property of the kernels with respect to the Caputo fractional derivative. To estimate a function’s Caputo fractional derivative, the function could be sampled and interpolated by linear combinations of Mittag-Leffler kernels, and then the Caputo fractional derivative could be estimated by multiplying the weights by the eigenvalues of the kernels. However, the Mittag-Leffler kernel functions have a singularity in their derivatives at the origin. This means that while convergence guarantees could be made in any neighborhood away from the origin, undesirable errors could still occur in a neighborhood of the origin.

In [11], this limitation was addressed in several ways. Particular to the approach of this manuscript, convergence guarantees were given in [11, Theorem 2.5], where continuous differentiability of a kernel function of a

degree higher than that of the fractional derivative allows convergence of the fractional derivatives of kernel based interpolants to that of the interpolated function. Theorem 3.1 provides an improvement over [11, Theorem 2.5] for the particular case of the Wendland RBF kernels. Theorem 3.1 follows immediately from Theorem 2.1.

**THEOREM 3.1.** *For  $d, r \in \mathbb{N}$ , let  $\Phi_{d,r} = \phi_{d,r}(\|\cdot\|)$  be a Wendland RBF. Further let  $I \subset \mathbb{R}$  be a compact interval. Let  $s_{f,X}$  be the RBF interpolant, determined by  $\Phi_{d,r}$ , to  $f$  in the RBFs native space over  $I$ ,  $N_{\Phi_{d,r}}(I)$ , and  $X = \{x_1, \dots, x_N\}$ . Fix  $q \in \mathbb{R}_+$  such that  $\alpha = \lceil q \rceil$  and  $\alpha < k$ . There exists constants  $C, h_0 > 0$  such that*

$$|D_*^q f(x) - D_*^q s_{f,X}(x)| \leq Ch_{X,I}^{r+1/2-\alpha} \|f\|_{N_{\Phi}(I)}$$

for all  $x \in I$  provided that  $h_{X,I} := \sup_{y \in I} \inf_{x \in X} \|x - y\| < h_0$ .

**P r o o f.** Write

$$D_*^q f(x) - D_*^q s_{f,X}(x) = \frac{1}{\Gamma(\alpha - q)} \int_0^x (x - \tau)^{\alpha - q - 1} \left( \frac{d^\alpha}{d\tau^\alpha} f(\tau) - \frac{d^\alpha}{d\tau^\alpha} s_{f,X}(\tau) \right) d\tau, \quad (3.1)$$

and note that the term inside of the parentheses of (3.1) can be estimated as in Theorem 2.1. Theorem 3.1 then follows by recognizing that the function  $\omega(x) := \int_0^x (x - \tau)^{\alpha - q - 1} d\tau$  is well defined, increasing, and bounded over  $I$ .  $\square$

Considering Theorem 3.1 and the subsequent Theorem 5.2, it can be seen that the Wendland RBF kernels have an advantage over the Mittag-Leffler kernels in establishing convergence rate estimates for both estimates of a function's fractional derivative as well as for the KPC method for FODEs. In particular, the Wendland RBF kernel functions do not suffer the same drawbacks near the origin as that of the Mittag-Leffler kernel functions.

Figure 1 presents an example demonstrating the differences in the performance of the Mittag-Leffler kernel function and that of the Wendland RBF interpolants in estimating the fractional derivative of the sine function with wavelength 1. A large error committed by the Mittag-Leffler interpolant can be observed near the origin. A heuristic explanation for this discrepancy is two fold. The Gram matrix used to interpolate the data quickly becomes ill-conditioned for dot product kernels, which leads to errors in the interpolating weights. These errors are amplified near the origin where each non-constant Mittag-Leffler has a vertical asymptote when  $0 < q < 1$ . Both figures set  $q = 1/4$ , and Figure 1(a) set  $T = 1$  and

$h = 0.005$  (the figure is zoomed on the interval  $[0, 0.1]$ ), whereas Figure 1(b) set  $T = 2$  and  $h = 0.01$ .

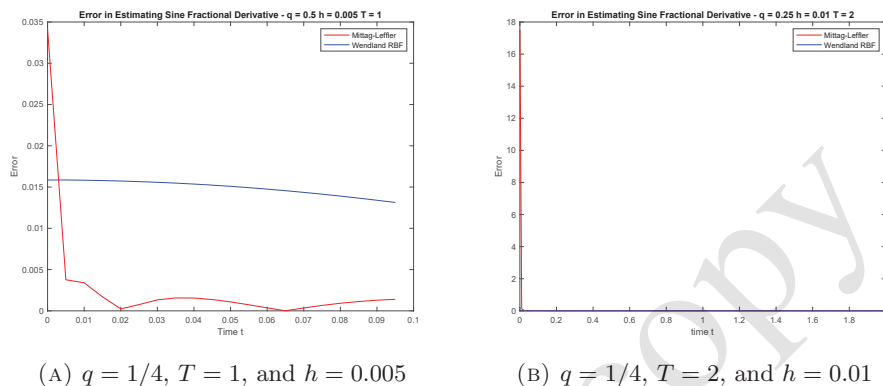


FIGURE 1. This figure shows the error committed by the Mittag-Leffler kernel and the Wendland RBF kernel interpolants in the estimation of the fractional derivative of the sine function. The fractional derivative of the sine function was independently computed using the power series representation of the function. It can be seen in both figures that the error committed in the estimation is poor near the origin for the Mittag-Leffler kernel function where it is as large as 18 units in Figure 1(b), while the Wendland RBF reports a consistent error bound.

#### 4. Description of the algorithm

The KPC method developed in [11] is a predictor corrector method that occurs in two steps. After the selection of collocation points,  $\{t_j\}_{j=0}^n \subset [0, T]$ , the algorithm begins by computing a predictor

$$y_{k+1}^P = \sum_{j=0}^{[q]} \frac{t_{k+1}^j}{j!} y_0^{(j)} + \frac{1}{\Gamma(q)} \sum_{j=0}^k b_{j,k+1} f(t_j, y_j), \quad (4.1)$$

where  $b_{j,k+1}$  arise from using a piecewise constant estimation of the integral in (1.2). For the particular case of equispaced points with spacing  $h > 0$  (i.e.  $t_j = jh$ ),  $b_{j,k+1} = \frac{h^q}{q} ((k+1-j)^q - (k-j)^q)$  as in [4].

The corrector in [4] is a piecewise linear interpolation of the data. In this manuscript, the corrector arises from RBF interpolants and is computed as

$$y_{k+1} = \sum_{j=0}^{[q]} \frac{t_{k+1}^j}{j!} y_0^{(j)} + \frac{1}{\Gamma(q)} \sum_{j=0}^{k+1} w_j \int_0^{t_{k+1}} (t_{k+1} - s)^{q-1} K(s, t_j) ds, \quad (4.2)$$

where  $K$  is a positive definite kernel function (cf. [11, 13, 14]) and  $\mathbf{w} = (w_0, \dots, w_{k+1})^T$  solves the matrix equation

$$(K(t_i, t_j))_{i,j=0}^{k+1} \mathbf{w} = \mathbf{f} \quad (4.3)$$

with  $\mathbf{f} = (f(t_0, y_0), f(t_1, y_1), \dots, f(t_k, y_k), f(t_{k+1}, y_{k+1}^P))^T$ .

To facilitate the development of an error bound of the form  $O(h^{k+1/2})$ , the algorithm is further modified by including a P(EC) $^\mu$ E method introduced in [4]. The P(EC) $^\mu$ E algorithm is a predictor corrector method where the corrector is iterated  $\mu$  times to improve accuracy. The predictor,  $y_{k+1}^{[0]} = y_{k+1}^P$  is used as the initial condition for the following recursive definition:

$$y_{k+1}^{[l]} = \beta_{k+1} + \frac{1}{\Gamma(q)} f(t_{k+1}, y_{k+1}^{[l-1]}) \int_0^{t_{k+1}} (t_{k+1} - s)^{q-1} u_{k+1}^*(s) ds, \quad (4.4)$$

where

$$\beta_{k+1} = \sum_{j=0}^{[q]} \frac{t_{k+1}^j}{j!} y_0^{(j)} + \frac{1}{\Gamma(q)} \sum_{j=0}^k f(t_j, y_j) \int_0^{t_{k+1}} (t_{k+1} - s)^{q-1} u_j^*(s) ds.$$

The quantity  $y^{[l]}$  is called the  $l$ -th corrector iteration.

Thus, the algorithm is completely described and results in the numerical solution to (1.1) given by  $\{(t_0, y_0), (t_1, y_1), \dots, (t_n, y_n)\}$  after  $n$  iterations.

## 5. Error analysis

This section establishes a big-oh estimate for the local truncation error of the KPC method when the Wendland RBFs are employed. The subsequent error analysis requires the establishment of convergence rates related to both the predictor and the corrector steps of the algorithm outlined in Section 4. Since the predictor is identical to that in [4], the following inequality found in [4, Theorem C.1] will be exploited, and in particular, the inequality corresponds to equally spaced points  $t_j = jh = j \cdot \frac{T}{n}$ .

**THEOREM 5.1** ([4]). *Let  $z \in C^1[0, T]$ . Then,*

$$\left| \int_0^{t_{k+1}} (t_{k+1} - \tau)^{q-1} z(\tau) d\tau - \sum_{j=0}^k b_{j,k+1} z(t_j) \right| \leq \frac{1}{q} \|z'\|_\infty t_{k+1}^q h.$$

Lemma 5.1 is a slight alteration of the results found in [3] and is necessary for demonstrating the convergence rate estimates for the corrector steps in Theorem 5.2.

LEMMA 5.1. *If  $p \geq 1$ ,  $\Omega \subset \mathbb{R}^d$  satisfying the interior cone condition, then for quasi-uniform spaced points,  $\|u_i^*\|_{L^p(\Omega)} \leq Ch^{d/p}$ .*

P r o o f. Since  $u_i^*$  is a linear combination of continuous compactly supported functions,  $u_i^* \in L^p$  for every  $p$ . The theorem then follows from the proof of the  $L^2$  bound in [3] where 2 is replaced by  $p \geq 1$ .  $\square$

THEOREM 5.2. *Set  $d, r \in \mathbb{N}$  and let  $f(\cdot, y(\cdot)) \in \mathcal{N}_{\Phi_{d,r}}$  and suppose that  $f$  is Lipschitz continuous. For  $q > 1$ , the  $P(EC)^rE$  algorithm given in (4.4) with the kernel function  $\Phi_{d,r}$  commits an error of*

$$|y(t_i) - y_i| \leq Ch^{r+1/2}.$$

P r o o f. As in the proof of [4, Lemma C.3], this proof will proceed by induction on  $i$ . For  $i = 0$ , the theorem follows automatically via the initial conditions. Now suppose that  $|y(t_i) - y_i| \leq Ch^{r+1/2}$  for  $i = 0, \dots, k$ .

For  $l \in \mathbb{N}$  take  $\hat{f}_{k+1}^{[l]}(s) = \sum_{i=0}^k f(t_i, y_i)u_i^*(s) + f(t_{k+1}, y_{k+1}^{[l]})u_{k+1}^*(s)$ . From [14] and the Lipschitz continuity of  $f$ , it can be seen that

$$\begin{aligned} & \left| f(s, y(s)) - \hat{f}_{k+1}^{[l]}(s) \right| \leq \left| \left\langle f, K(\cdot, s) - \sum_{i=0}^{k+1} u_i^*(s)K(\cdot, t_i) \right\rangle \right| \\ & + \sum_{i=0}^{k+1} |f(t_i, y(t_i)) - f(t_i, y_i)| |u_i^*(s)| + |f(t_i, y(t_i)) - f(t_{k+1}, y_{k+1}^{[l]})| |u_{k+1}^*(s)| \\ & \leq C\|f\|h^{k+1/2} + L \sum_{i=0}^k |y(t_i) - y_i| |u_i^*(s)| + L|y(t_{k+1}) - y_{k+1}^{[l]}| |u_{k+1}^*(s)|. \end{aligned}$$

Now consider,

$$|y(t_{k+1}) - y_{k+1}^{[l]}| \leq (C\|f\|h^{k+1/2}) \int_0^{t_{k+1}} (t_{k+1} - s)^{q-1} ds$$

$$\begin{aligned}
& + L \sum_{i=0}^k |y(t_i) - y_i| \int_0^{t_{k+1}} (t_{k+1} - s)^{q-1} |u_i^*(s)| ds \\
& + L |y(t_{k+1}) - y_{k+1}^{[l-1]}| \int_0^{t_{k+1}} (t_{k+1} - s)^{q-1} |u_{k+1}^*(s)| ds \\
& \leq C_1 \|f\| h^{k+1/2} + LC_2 h^{k+1/2} M_{k+1} \sum_{i=0}^k \|u_i^*(s)\|_{L^1[0,T]} \\
& + L |y(t_{k+1}) - y_{k+1}^{[l-1]}| M_{k+1} \|u_{k+1}^*(s)\|_{L^1[0,T]} \\
& \leq C_1 \|f\| h^{r+1/2} + LMC_2 h^{r+1/2} (k+1)h \\
& + LMC_3 h |y(t_{k+1}) - y_{k+1}^{[l-1]}| \\
& \leq C_1 \|f\| h^{r+1/2} + LMC_2 T h^{r+1/2} \\
& + LMC_3 h |y(t_{k+1}) - y_{k+1}^{[l-1]}|,
\end{aligned}$$

where each constant  $C_1, C_2, L > 0$  and are independent of  $h$  and  $k$ . Writing  $P_l = |y(t_{k+1}) - y_{k+1}^{[l]}|$  the following recursive inequality is established  $P_l \leq C_1 h^{r+1/2} + C_2 h P_{l-1}$ . Therefore,

$$P_r \leq Ch^{r+1/2} + Dh^r P_0 \leq Ch^{r+1/2} + \tilde{D}h^{r+1},$$

with  $C, D, \tilde{D} > 0$  and independent of  $h$  and  $k$ . Note that  $P_0 = O(h)$  follows from Theorem 5.1, since  $f(\cdot, y(\cdot)) \in C^1[0, T]$ . Also note  $M_{k+1} := \sup_{s \in [0, t_{k+1}]} (t_{k+1} - s)^{q-1} = t_{k+1}^{q-1}$ , and  $M = \max_k M_k = T^{q-1}$ . Thus,  $|y(t_{k+1}) - y_{k+1}^{[r]}| = P_r \leq Ch^{r+1/2}$  and the induction argument is complete.  $\square$

## 6. The fractional integral of the Wendland functions

It is clear from the results in Section 5 that to leverage the KPC method, it is necessary to compute or estimate the fractional integral of the selected kernel function. The Wendland functions are an ideal choice for approximating the solution to a fractional differential equation, since Wendland RBFs are compactly supported and are polynomials on their support. Therefore, the fractional integrals of Wendland RBFs can be computed in closed form using integration by parts on each monomial constituent of the Wendland RBFs, whose coefficient can be determined recursively as described in [14, Theorem 9.12].

Since each kernel function,  $K(\tau, t_i)$ , is a function of the time variable,  $\tau$ , the integral may be split across the interval about the point  $\tau = t_i$ . That

is, the fractional integral can be written as

$$\begin{aligned} & \frac{1}{\Gamma(q)} \int_0^s (s - \tau)^{q-1} K(\tau, t_i) d\tau \\ &= \frac{1}{\Gamma(q)} \left( \int_0^{t_i} (s - \tau)^{q-1} \Phi_{d,r}(|\tau - t_i|) d\tau + \int_{t_i}^s (s - \tau)^{q-1} \Phi_{d,r}(|\tau - t_i|) d\tau \right) \\ &= \frac{1}{\Gamma(q)} \left( \int_0^{t_i} (s - \tau)^{q-1} \Phi_{d,r}(t_i - \tau) d\tau + \int_{t_i}^s (s - \tau)^{q-1} \Phi_{d,r}(\tau - t_i) d\tau \right), \end{aligned}$$

and each of  $\Phi_{d,r}(t_i - \tau)$  and  $\Phi_{d,r}(\tau - t_i)$  are polynomials on the support of  $\Phi_{d,r}$ . Indeed, since  $\Phi_{d,r}(|\tau - t_i|)$  is compactly supported on the interval  $[t_i - 1, t_i + 1]$ , the bounds on the integrals may be replaced, setting  $a = \max\{0, t_i - 1\}$  and  $b = \min\{s, t_i + 1\}$ , as

$$\frac{1}{\Gamma(q)} \left( \int_a^{t_i} (s - \tau)^{q-1} \Phi_{d,r}(t_i - \tau) d\tau + \int_{t_i}^b (s - \tau)^{q-1} \Phi_{d,r}(\tau - t_i) d\tau \right),$$

where the integrand is now strictly a polynomial. The bounds  $a$  and  $b$  may be adjusted if  $\Phi_{d,r}$  is scaled to different widths.

Specifically, it may be observed that for each  $m \in \mathbb{N}$ :

$$\begin{aligned} & \int_a^b (s - \tau)^{q-1} |\tau - t_i|^m d\tau \\ &= \int_a^{t_i} (s - \tau)^{q-1} (t_i - \tau)^m d\tau + \int_{t_i}^b (s - \tau)^{q-1} (\tau - t_i)^m d\tau \\ &= \sum_{j=0}^m \frac{m!}{(m-j)! \cdot q(q+1) \cdots (q+j)} Q_{a,b,i,j,m,q} \\ & \quad + \frac{m!}{q(q+1) \cdots (q+m+1)} \tilde{Q}_{s,a,b,m,q,i}, \text{ where} \\ Q_{a,b,i,j,m,q} &:= ((-1)^m (a - t_i)^{m-j} (s - a)^{q+j} - (b - t_i)^{m-j} (s - b)^{q+j}), \text{ and} \\ \tilde{Q}_{s,a,b,m,q,i} &:= ((-1)^m (s - a)^{q+m+1} + \\ & (1 + (-1)^{m+1})(s - t_i)^{q+m+1} - (t_k - b)^{q+m+1}). \end{aligned}$$

Thus, through a combination of the above computation for monomials and [14, Theorem 9.12], an explicit description of the fractional integrals of the Wendland RBFs may be obtained.

### 7. Numerical experiments

This section presents the numerical results from several fractional order IVPs using the KPC method. Each of the experiments has a corresponding known analytic solution (cf. [1, 4]), which enables the reporting of precise

errors committed by the KPC method. Moreover, the method of [4] is applied to the same IVPs for the purpose of comparison in Table 1. Figure 2 presents several representative examples of the KPC method and the method of [4]. These examples can be found in [1, 4].

The results of further experiments are displayed in Figure 3, where the errors committed by each of the above methods are displayed along with the errors committed by the KPC method using the Mittag-Leffler kernel from [11]. Figure 3 gives the errors in estimating the solution to the three subsequent examples plotted according to a selected step-size,  $h$ , ranging from 0.1 to 0.25. A log-log plot of the data in Figure 3 is presented in Figure 4, where empirical convergence orders may be inferred.

**EXAMPLE 1.** The first example is the most straightforward for fractional order IVPs,  $D_*^q y(s) = -y(s)$  with  $y(0) = 1$  for  $q > 0$ . The solution of this fractional order IVP is given with respect to the Mittag-Leffler function:  $y(s) = E_q(-s^q)$ .

**EXAMPLE 2.** The second example stems from [4], where the example is used as a benchmark for the ABM method of [4],

$$D_*^q y(s) = \frac{40320}{\Gamma(9-q)} s^{8-q} - 3 \frac{\Gamma(5+q/2)}{\Gamma(5-q/2)} s^{4-q/2} + \frac{9}{4} \Gamma(q+1) + \left(\frac{3}{2} s^{q/2} - s^4\right)^3 - (y(s))^{3/2}.$$

For  $0 < q < 2$ ,  $y(0) = 0$ , and  $y'(0) = 0$  (when  $q > 1$ ), the solution to this example is given as  $y(s) = s^8 - 3s^{4+q/2} + \frac{9}{4}s^q$ .

**EXAMPLE 3.** For  $q > 0$ , the third example is given as

$$D_*^q y(s) = 0.1s - y(s) \text{ with } y(0) = 1 \text{ and } y'(0) = 0.$$

The exact solution for this fractional order differential equation is given in terms of the Mittag-Leffler function of two parameters:

$$y(s) = 0.1s(1 - E_{q,s}(-s^q)) + E_{q,1}(-s^q),$$

where  $E_{\alpha,\beta}(s) := \sum_{n=0}^{\infty} \frac{s^n}{\Gamma(\alpha n + \beta)}$ .

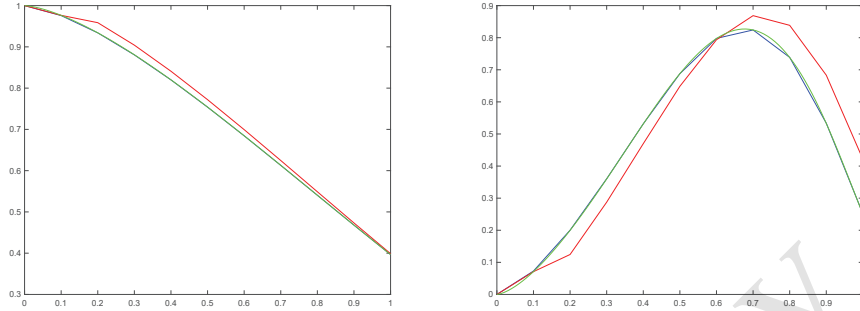
## 8. Discussion

Based on the results of Table 1 the KPC method outperforms the ABM method in [4] by as much as a factor of 1000 in Example 2 with  $q = 1.5$  and  $h = 0.025$ . However, when compared to the computation time of the ABM method of [4], the competing method outperforms the KPC method by a factor of 100 in computation time on that particular example. The

Ex. #	q	h	KPC	Time (s)	ABM	Time (s)
Ex. 1	0.50	0.100	1.6980E-2	2.3884E-1	2.9019E-2	5.7942E-4
		0.050	7.4314E-3	7.2242E-1	2.2630E-2	7.4421E-4
		0.025	3.5545E-3	2.5432E+0	1.7158E-2	1.5473E-3
	1.50	0.100	5.8448E-4	2.0686E-1	2.4579E-2	5.7714E-4
		0.050	5.3387E-5	6.8096E-1	8.8500E-3	8.3292E-4
		0.025	3.0367E-5	2.5552E+0	3.1491E-3	1.8033E-3
Ex. 2	0.50	0.100	1.1564E-2	2.2703E-1	5.9105E-2	1.3442E-3
		0.050	2.4083E-3	6.9801E-1	4.7279E-2	3.5073E-3
		0.025	4.6055E-4	2.6205E+0	3.6048E-2	1.0404E-2
	1.50	0.100	1.8502E-3	2.6522E-1	1.7140E-1	8.0984E-3
		0.050	1.7921E-4	7.8876E-1	5.6541E-2	4.4184E-3
		0.025	4.6735E-5	2.6347E+0	1.9915E-2	1.1452E-2
Ex. 3	0.50	0.100	1.6990E-2	2.0278E-1	2.8782E-2	8.6738E-4
		0.050	7.4395E-3	6.9359E-1	2.2533E-2	1.2485E-3
		0.025	3.5573E-3	2.5337E+0	1.7120E-2	1.6768E-3
	1.50	0.100	5.8212E-4	1.9352E-1	2.4329E-2	7.9372E-4
		0.050	5.3282E-5	8.0269E-1	8.8055E-3	1.0398E-3
		0.025	3.1615E-5	2.4497E+0	3.1412E-3	1.9239E-3

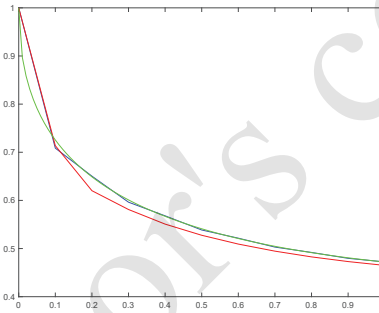
TABLE 1. This table presents the results of several numerical experiments performed on the examples outlined in Section 7 with fractional orders of  $q = 0.5$  and  $q = 1.5$  and step sizes ranging from  $h = 0.1$  to  $h = 0.025$  for an overall time period of  $T = 1$ . The KPC method (whose error at the time steps is presented in the KPC column of this table) was performed using the Wendland radial basis function  $\Phi_{3,6}$ . The KPC method is compared to the ABM method of [4]. Both methods used six corrector steps per time-step. It can be observed that the KPC method performs as much as 1000 times better than the ABM method in terms of accuracy, yet the KPC method performed worse in terms of computation time.

reason for the difference in computation time is the algorithmic complexity of the two methods. At each time step the KPC method must compute weights through the solution to a linear system of equations governed by the Gram matrix corresponding to the points  $h * j$  for  $j = 0, \dots, i$ . Solving this system of linear equations takes up to  $O(i^3)$  operations. For the ABM method of [4], the weights are explicitly described and it is not necessary



(A) Example 1 with  $q = 1.5$  and  $h = 0.1$ .

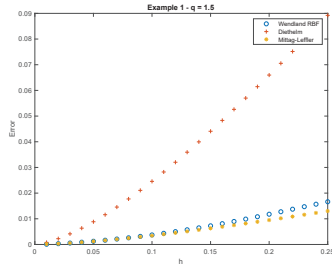
(B) Example 2 with  $q = 0.5$  and  $h = 0.1$ .



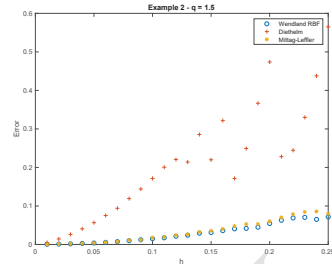
(C) Example 3 with  $q = 0.5$  and  $h = 0.1$ .

FIGURE 2. The results of three representative experiments are presented here. In each figure, the red trajectory represents the ABM method of [4], the blue trajectory represents the KPC method, and the green trajectory is the known exact solution for the corresponding example. The spacing selected for each experiment is  $h = 0.1$ , since the differences between the accuracy of the methods is most apparent at this resolution.

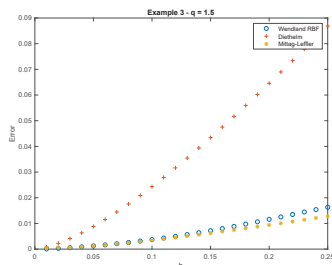
to recompute the weights at each step. Consequently, each step in the ABM method of [4] only requires  $O(i)$  operations. It should be noted that the results for the ABM method of [4] uses the algorithm given in [4]. More recent work such as [10] has introduced algorithms for the ABM method which improves upon the computational complexity of that found in [4]. Since the computation times found in Table 1 already differ greatly



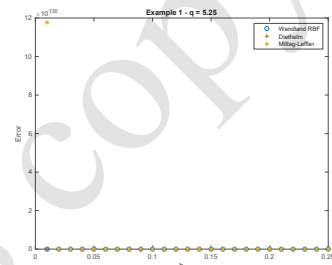
(A) Example 1:  $q = 1.5$



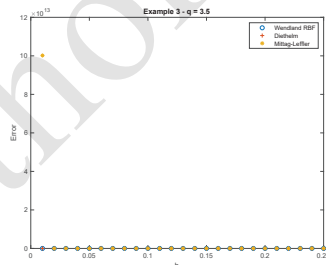
(B) Example 2:  $q = 1.5$



(C) Example 3:  $q = 1.5$



(D) Example 1:  $q = 5.25$



(E) Example 3:  $q = 3.5$

FIGURE 3. This figure shows the errors committed according to the step-size taken in the numerical method. In Section 7, three different numerical methods were utilized. These include, the KPC method using the Wendland RBFs developed in this manuscript (circles), the method of [4] (pluses), and the KPC method using the Mittag-Leffler kernel function (stars). Figure 3(a) through Figure 3(c) encompass the values presented for  $q = 1.5$  in Table 1, but also add error values corresponding to the Mittag-Leffler kernel. The KPC method using the Wendland RBF performed as well or better than both other methods asymptotically as  $h \rightarrow 0$ .

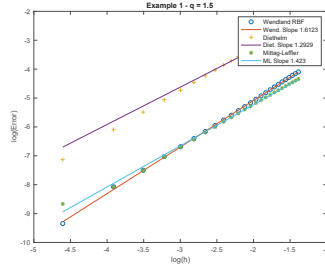
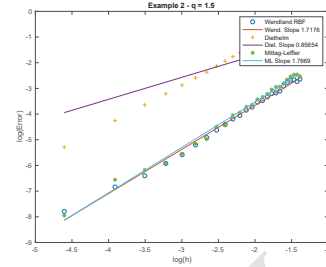
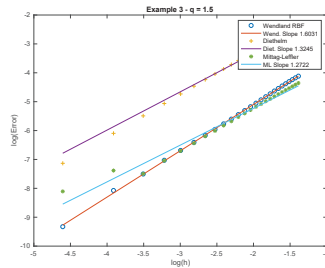
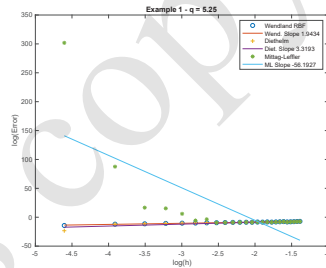
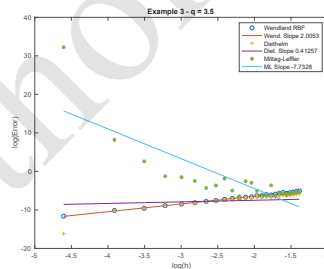
(A) Example 1:  $q = 1.5$ (B) Example 2:  $q = 1.5$ (C) Example 3:  $q = 1.5$ (D) Example 1:  $q = 5.25$ (E) Example 3:  $q = 3.5$ 

FIGURE 4. This figure displays a log-log plot corresponding to Figure 3. Here the log of the error data is plotted against the logarithm of  $h$ . For each collection of data points, a best fit line is plotted as determined by a least squares fit. The slope of each line gives an empirical estimate of the convergence order. With the exception of Figure 4(d) and Figure 4(e), it can be observed that both the KPC method using the Mittag-Leffler kernel and the Wendland RBF outperforms that of Diethelm's method. However, in Figure 4(d) and Figure 4(e), it can be observed that the Mittag-Leffler kernel function performs poorly.

between the KPC and the ABM method as implemented according to [4], the implementation of more sophisticated algorithms is unnecessary for the demonstration of the gap in computation time between the methods.

The expense of computational complexity yields improved performance. Specifically, using the same number of samples of the dynamical systems, the kernelized method performed much better than the ABM method of [4]. Heuristically, the better performance arises from the smoothness of the Wendland basis functions, where in approximation theory, the approximation order is governed by the regularity of the target function and the basis functions selected. This heuristic is supported by Theorem 5.2 in the present manuscript.

The results of Theorem 5.2 can be extended to a larger class of kernel functions than that of the Wendland radial basis functions. In particular, the necessary property for the successful application of the corrector steps lies in the Lebesgue constant for cardinal functions,  $|\sum_{i=1}^N u_i^*(x)| < C\sqrt{N}$ , which is described in [3]. This bound extends to a larger class of basis functions, which are also described in [3], of which Wendland RBFs are the most well known examples.

Figure 3 presents the results of further experiments where  $h$  takes on more values than presented in Table 1 for  $q = 1.5$ , and shows error values for larger values of  $q$ . Additionally, experiments utilizing the Mittag-Leffler kernel function were included. In each experiment the Wendland RBF matches or outperforms the other methods asymptotically as  $h \rightarrow 0$ . The KPC method using the Mittag-Leffler kernel function frequently matched the accuracy of that with the Wendland RBF, especially in Example 2. However, for several values of  $h$  it can be observed that the KPC method using the Mittag-Leffler kernel function generated significantly large errors. In fact, the ranges of  $h$  values for Figure 3(d) and Figure 3(e) begin at different  $h$  values of  $h = 0.07$  and  $h = 0.05$  respectively. For smaller values of  $h$  the KPC method using the Mittag-Leffler kernel functions generated dramatically large and unpredictable errors. Heuristically, the infinite smoothness of the Mittag-Leffler functions over  $(0, \infty)$  make them an ideal candidate for kernel functions that would allow for a faster convergence rate than the Wendland RBFs, which are only continuously differentiable for a finite number of derivatives. However, numerical implementation of the Mittag-Leffler kernel function in the KPC method requires the evaluation of expressions of the form  $\frac{1}{\Gamma(q)} \int_0^s (s-t)^{q-1} E_q(\lambda^q t^q) dt = \frac{1}{\lambda^q} E_q(\lambda^q s^q)$  for  $\lambda$  near zero. Therefore, any numerical errors in the weights will be amplified when  $\lambda$  is near zero, as when a center is placed at a time step near the origin. Thus, Figure 3 establishes the use of the KPC method with the

Wendland RBFs as a more accurate and consistent method than that of the competitors.

The empirical convergence rates that can be inferred from the slopes of the lines found in Figure 4 for the Wendland RBF are smaller than the theoretical convergence rates found in Theorem 5.2 given the Wendland RBF used corresponds to  $\Phi_{3,6}$ . One possible explanation for Example 2 and Example 3 is that the dynamics are both not smooth enough to accommodate the hypothesis of Theorem 5.2.

## 9. Conclusion

This manuscript presented a KPC method for the generation of solutions to Caputo fractional order IVPs. The innovation beyond the existing KPC algorithm in [11] is that a convergence rate estimate is established in terms of a power of the step size,  $h$ , by utilizing properties of the Wendland RBFs. In addition, the use of the Wendland RBFs over the Mittag-Leffler kernel functions removes the problems in the KPC method encountered near the origin in [11], and this improvement is demonstrated in Figure 1, Figure 3, and Figure 4. The resulting numerical algorithm was compared to an existing fractional order ABM algorithm that can be found in [4] on several benchmark examples, and the results of which are shown in Table 1, Figure 3, and Figure 4. The kernelized method using the Wendland RBF outperformed the methods of [4] and [11] in terms of accuracy, but had inferior performance to [4] in computation time.

## Acknowledgments

The work of the authors was supported in part by NSF award 1509516 and Office of Naval Research grant N00014-13-1-0151. The first author was further supported by the Air Force Office of Scientific Research (AFOSR) under contract numbers FA9550-15-1-0258, FA9550-16-1-0246, FA9550-18-1-0122, and FA9550-21-1-0134 during the preparation of the manuscript. Any opinions, findings, and conclusions or recommendations expressed in this material are those of the authors and do not necessarily reflect the views of the sponsoring agencies.

## References

- [1] O. P. Agrawal and P. Kumar, Comparison of five numerical schemes for fractional differential equations. In: *Advances in Fractional Calculus*, Springer, 2007, 43–60.
- [2] N. Aronszajn, Theory of reproducing kernels. *Trans. Amer. Math. Soc.* **68** (1950), 337–404, DOI: 10.2307/1990404.

- [3] S. De Marchi and R. Schaback, Stability of kernel-based interpolation. *Adv. in Computational Math.* **32** (2010), 155–161; DOI: 10.1007/s10444-008-9093-4.
- [4] K. Diethelm, *The Analysis of Fractional Differential Equations: An Application-Oriented Exposition Using Differential Operators of Caputo Type*. Springer, 2010.
- [5] K. Diethelm and N. J. Ford, Analysis of fractional differential equations. *J. of Math. Anal. and Appl.* **265** (2002), 229–248.
- [6] K. Diethelm and N. J. Ford, Multi-order fractional differential equations and their numerical solution. *Appl. Math. and Computation* **154** (2004), 621–640.
- [7] K. Diethelm, N. J. Ford, and A. D. Freed, A predictor-corrector approach for the numerical solution of fractional differential equations. *Nonlin. Dynamics* **29** (2002), 3–22.
- [8] L. C. Evans, *Partial Differential Equations*. Graduate Studies in Mathematics, Vol. 19, Amer. Math. Soc., 1998.
- [9] G. E. Fasshauer, *Meshfree Approximation Methods with Matlab (With CD-ROM)*, Vol. 6. World Scientific Publishing Company, 2007.
- [10] R. Garrappa, Numerical solution of fractional differential equations: A survey and a software tutorial. *Mathematics* **6**, No 2 (2018), 16 pp.; DOI: 10.3390/math6020016.
- [11] J. A. Rosenfeld and W. E. Dixon, Approximating the Caputo fractional derivative through the Mittag-Leffler reproducing kernel Hilbert space and the kernelized Adams–Bashforth–Moulton method. *SIAM J. on Numer. Anal.* **55** (2017), 1201–1217.
- [12] J. A. Rosenfeld, B. Russo, and W. E. Dixon, The Mittag-Leffler reproducing kernel Hilbert spaces of entire and analytic functions. *J. of Math. Anal. and Appl.* **463** (2018), 576–592.
- [13] I. Steinwart and A. Christmann, *Support Vector Machines*. Springer Sci. & Business Media, 2008.
- [14] H. Wendland, *Scattered Data Approximation*, Vol. 17. Cambridge University Press, 2004.

<sup>1</sup> *The Learning DOCK Group*  
*Department of Mathematics and Statistics*  
*University of South Florida, Tampa, FL 33620 - USA*  
*e-mail: rosenfeldj@usf.edu (Corresponding author)*

*Received: June 18, 2019, Revised: October 24, 2021*

<sup>2</sup> *Nonlinear Controls and Robotics (NCR) Laboratory*  
*Department of Mechanical and Aerospace Engineering*  
*University of Florida, Gainesville, FL 32611 - USA*  
*e-mail: wdixon@ufl.edu*

---

Please cite to this paper as published in:

*Fract. Calc. Appl. Anal.*, Vol. **24**, No 6 (2021), pp. 1879–1898,  
DOI: 10.1515/fca-2021-0081

Author's copy